Simulation studies on ion acceleration driven by 10 PW laser

M. Matys[1], J. Psikal[1,2], D. Margarone[2]

[1] *FNSPE, Czech Technical University in Prague, Prague, Czech Republic*

[2] *ELI-Beamlines project, Institute of Physics, AS CR, Prague, Czech Republic*

Ultrashort laser facilities currently built will be able to deliver up to 10 PW peak power, e.g., L4 beamline (1.5 kJ, 150 fs pulses) in the frame of ELI-Beamlines project [1]. The interaction of such ultrahigh intensity laser beam with ionized solid targets includes many new phenomena such as relativistic transparency [2] or substantial energy losses of electrons oscillating in the laser wave by radiation reaction force (RR) [3]. We studied the interaction with the help of numerical 2D3V particle-in-cell simulations including QED module calculating radiation reaction of electrons by MC approach [4]. Namely, laser-driven ion acceleration is investigated for laser parameters relevant to the L4 ELI beamline and for newly developed hydrogen solid cryogenic target with thickness down to 25 μm [5] and standard polyethylene foil with thickness down to 5 μm.

All simulated laser pulses are linearly p-polarised, incident normally on the target and have diameter of 5 μm (at FWHM), wavelength 1100 nm and pulse duration 150 fs (approximated by 320 fs full $\sin^2$ pulse). Laser peak intensity of 3×10^{22} W/cm^2 was used to compare simulations with hydrogen and polyethylene targets, while intensities varying from 1.5×10^{22} W/cm^2 to 0.375×10^{22} W/cm^2 were used for simulations with hydrogen target only. Both targets are fully ionized with electron density 56.2 n_c in the case of hydrogen target and 339.2 n_c in the case of polyethylene target, respectively. Where n_c is the critical density.

Despite its low density, the cryogenic hydrogen target still does not become transparent to the simulated laser pulse and hole boring radiation pressure acceleration mechanism (HB RPA) occurs in our simulations alongside with the target normal sheath acceleration (TNSA). With the use of high intensities, the radiation reaction force appreciably affects both these acceleration mechanisms and causes the decrease of maximum proton energy and a shift of whole proton energy spectra to lower energies as can be seen in Fig. 1. Moreover, an interesting region occurs in the energy range 175-250 MeV,

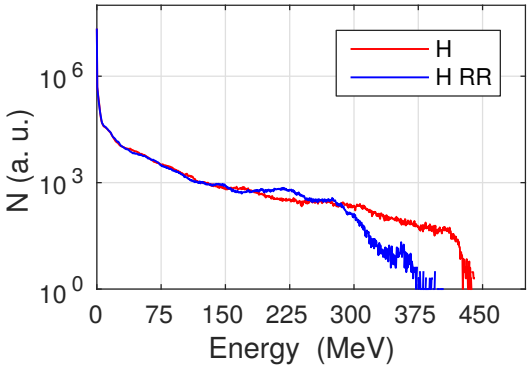

Figure 1: *Proton energy spectra at time instant 190 fs in the simulation of hydrogen target with and without radiation reaction force.*

where more protons are counted in the case with RR than in the case without RR. This phenomenon can be explained by the difference in the motion of the electrons from the interaction area, e.g. the backward motion of the electrons is slowed down by the interaction with laser pulse, as it was shown for thin (1 μm) targets [6].

Combination of high laser intensities and low target densities demonstrated the importance of RPA mechanism which accelerated more fast protons (with energy over 10 MeV) than TNSA at the time instances, when the influence of these two mechanisms can be still clearly distinguished (as can be seen in Fig. 2), in all simulation cases. In the case of hydrogen target, the ratio of fast protons accelerated by RPA and TNSA is decreasing with intensity from 9 times more in the case of intensity 3×10^{22} W/cm^2 to 2 times more for intensity 0.375×10^{22} W/cm^2. At the corresponding time instances RPA mechanism accelerates protons to higher maximum energy than TNSA for intensity range from 3×10^{22} W/cm^2 to 0.75×10^{22} W/cm^2, however for the simulation with intensity 0.375×10^{22} W/cm^2 the maximum energy of protons accelerated by RPA is lower than by TNSA. On the contrary, in the case of polyethylene target, the number of fast protons accelerated by RPA and TNSA is only 1.7 times more already at intensity 3×10^{22} W/cm^2 and RPA mechanism also accelerates protons to lower maximum energies than TNSA (Fig. 2b). Both of this phenomena correspond to much higher density of polyethylene target and larger mass of its ions, therefore the hole boring velocity is slower and RPA mechanism is less efficient.

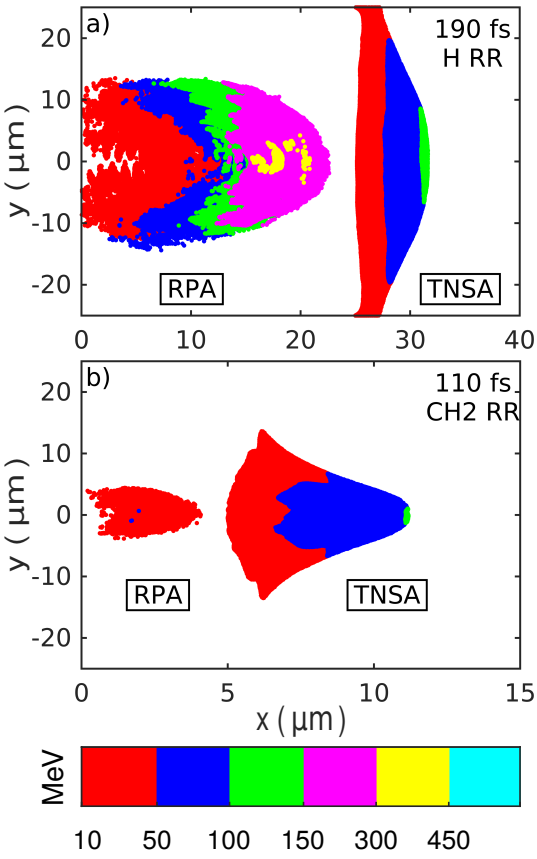

Figure 2: *Proton energy layers in the simulations with a) hydrogen and b) polyethylene targets.*

At the later time the protons previously accelerated by RPA reach the rear side of the target and are subsequently accelerated by the TNSA field. Separation of protons with energy in range 225-300 MeV (green) accelerated by pure TNSA (denoted as 1) and this mixture RPA/TNSA mechanism (denoted as 2) is still clearly visible at the late time of simulation (340 fs) in Fig. 3a).

After the laser pulse burns through the target, another distinguishable mechanism arises from

the laser interaction with the target debris, which is still overdense, but become relativistically transparent. These conditions lead to more efficient volumetric acceleration of electrons [7], while there are still enough electrons to efficient coupling with protons [8]. This mechanism, denoted as 3 in Fig. 3a), further accelerates a relatively small fraction of protons to energy over 600 MeV (cyan), while other mechanisms accelerates protons under 400 MeV (magenta), in the case of CH2 target. This mechanism also accelerates protons to highest energy in the case of hydrogen target (Fig. 3b). In Fig. 3c) the proton energy spectra are shown. The maximum energy of protons accelerated from the hydrogen target (blue) is near the maximum energy of protons originated from the polyethylene target (green), however the number of accelerated high-energy protons is substantially higher in the case of hydrogen target. This phenomenom is caused by the different efficiency of hole boring mechanism. In the case of hydrogen target (Fig. 3b), only about 53% of protons accelerated over 400 MeV (yellow) are located inside the black rectangle, which surrounds the area, where the laser pulse propagating through the debris is located. Therefore about 47 % of these protons are accelerated by the mixture RPA/TNSA mechanism. On the contrary, the corresponding area in Fig. 3b (denoted as 3) contains 100 % of this type of protons in the case of polyethylene target.

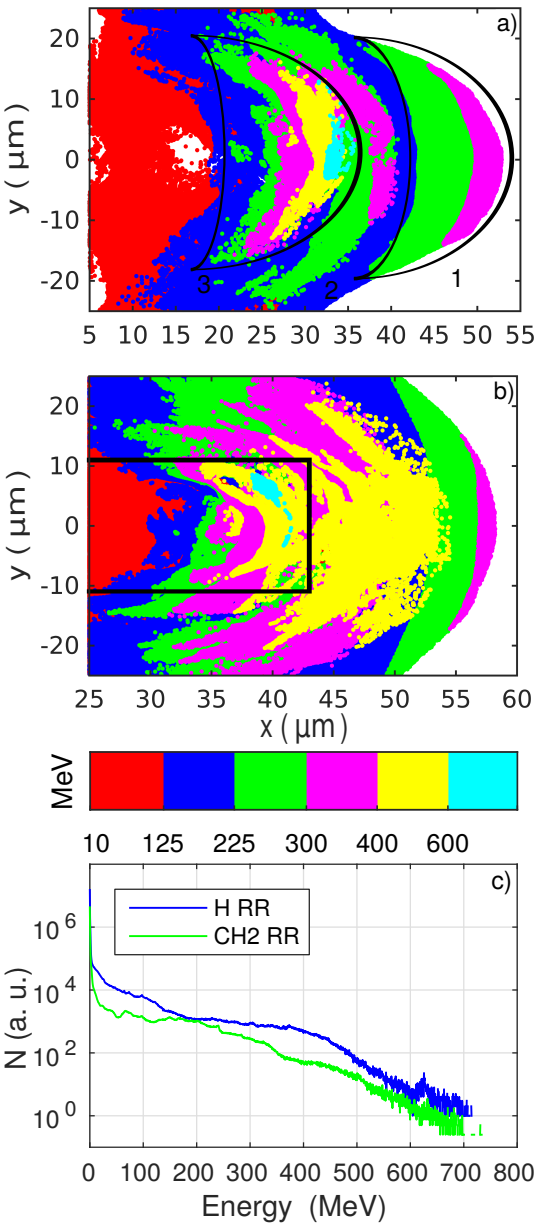

Figure 3: *Proton energy layers in the simulations with a) hydrogen and b) polyethylene targets and c) proton energy spectra at time instant 340 fs.*

To better understand the acceleration mechanisms in interaction with lower laser intensities, more simulations were produced in the case of hydrogen target. Maximum energy of different mechanisms are shown in Fig. 4. The mechanism of laser-debris interaction was observed only in the simulations with laser intensity high enough to burn through the target, i.e. 3×10^{22} W/cm^2 and 1.5×10^{22} W/cm^2 and accelerated pro-

tons to significantly higher energy than TNSA. In the case of intensity 0.75×10^{22} W/cm^2, mixture RPA/TNSA mechanism accelerates protons to energies similar to TNSA and in the case of intensity 0.375×10^{22} W/cm^2, mixture RPA/TNSA mechanism almost did not occurred and TNSA mechanism accelerated protons to highest energies.

In conclusion, the produced simulations of high intensity laser pulse with cryogenic hydrogen and polyethylene targets proved the necessity of QED module in this type of interaction and importance of RPA mechanism in interactions with the low density target. Although the maximum energy of protons accelerated from these two targets reached similar values, the number of accelerated high-energy protons is substantially higher in the case of hydrogen target. Therefore this target is theoretically more suitable for laser-driven acceleration. The simulations with lower intensities showed the strong influence of non purely TNSA mechanisms till intensity 0.75×10^{22} W/cm^2 ($\approx$ 2 PW laser power), which accelerated protons to energies over 200 MeV.

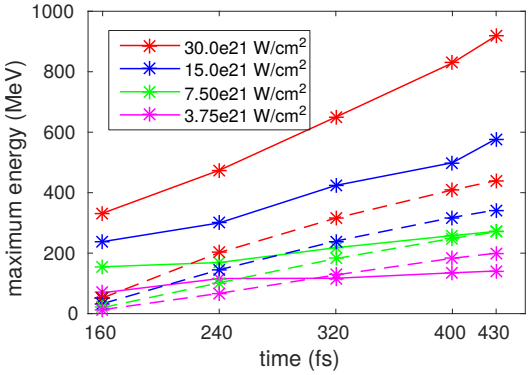

Figure 4: *Time evolution of maximum proton energy in simulations with different laser intensities. Solid and dashed lines denote RPA/mixtures and pure TNSA mechanisms, respectively.*

This research has been partially supported by the Czech Science Foundation (Project No. 15- 02964S). Computational resources were supplied by the Ministry of Education, Youth and Sports of the Czech Republic under the Projects CESNET (Project No. LM2015042) and CERIT-Scientific Cloud (Project No. LM2015085) provided within the program Projects of Large Research, Development and Innovations Infrastructures.

References

[1] ELI Beamlines, www.eli-beams.eu; G. Mourou, G. Korn, W. Sandner, and J. L. Collier, ELI Whitebook (Andreas Thoss, Berlin, 2011);

[2] A. Macchi, A Superintense Laser-Plasma Interaction Theory Primer, Springer Netherlands, (2013)

[3] L. Landau and E. Lifshitz, The Classical Theory of Fields, Pergamon Amsterdam, (1975)

[4] T. D. Arber, K. Bennett, C. S. Brady *et al.*, Plasma Phys. Control. Fusion **57**, 113001 (2015)

[5] D. Margarone, A. Velyhan, J. Dostal *et al.*, Phys. Rev. X **6**, 041030 (2016)

[6] M. Tamburini, F. Pegoraro, A. D. Piazza *et al.*, Nuclear Inst. and Methods in Physics Research **653**, 1 (2011)

[7] D. Jung, L. Yin, B. J. Albright *et al.*, New Journal of Physics **15**, 023007 (2013)

[8] B. M. Hegelich, I. Pomerantz, L. Yin *et al.*, New Journal of Physics **15**, 085015 (2013)